



Metabolism of SKLB-TB1001, a Potent Antituberculosis Agent, in Animals

Lu Xiong,^a Chao Gao,^a Yao-Jie Shi,^a Xin Tao,^a Cui-Ting Peng,^{a,b} Juan Rong,^a Kun-Lin Liu,^a Qian Lei,^a Yi-Wen Zhang,^a Ning-Yu Wang,^c Luo-Ting Yu^a

^aState Key Laboratory of Biotherapy and Cancer Center, West China Hospital, Sichuan University and Collaborative Innovation Center, Chengdu, China

^bDepartment of Pharmaceutical and Bioengineering, School of Chemical Engineering, Sichuan University, Chengdu, Sichuan, China

^cSchool of Life Science and Engineering, Southwest JiaoTong University, Sichuan, China

ABSTRACT Tuberculosis is a major global health problem, and the emergence of multidrug-resistant and extensively drug-resistant strains has increased the difficulty of treating this disease. Among the novel antituberculosis drugs in the pipeline, decaprenylphosphoryl-beta-D-ribose-2-epimerase (DprE1) inhibitors such as BTZ043 and pBTZ169 exhibited extraordinary antituberculosis potency. Here, the metabolites of the new DprE1 inhibitor SKLB-TB1001 *in vivo* and its inhibition of cytochrome P450 isoforms and plasma protein binding (PPB) *in vitro* were studied. The results showed that rapid transformation and high PPB resulted in inadequate exposure *in vivo* and thus led to the moderate potency of SKLB-TB1001 *in vivo*. This study provided explanations for the discrepant potency of this scaffold *in vivo* and *in vitro*. Meanwhile, it also provides a rationale for lead optimization of this very promising scaffold of antituberculosis agents to prevent them from being metabolized, thus improving their exposure *in vivo*.

KEYWORDS DprE1, MDR-TB, drug metabolism, tuberculosis

Tuberculosis (TB) is an infectious disease caused by *Mycobacterium tuberculosis*, and it was one of the leading causes of death by the beginning of the twentieth century (1). With an estimated 1.4 million deaths and 11 million new cases in 2016 (http://www.who.int/tb/publications/global_report/archive/en/), this disease is a serious threat to human health. Currently, the standard curative treatment for patients with tuberculosis is a four-drug cocktail composed of rifampin (RIF), isoniazid (INH), pyrazinamide, and ethambutol. This is followed by a longer phase of treatment with RIF and INH to eradicate the remaining bacilli, which are present in a dormant, slowly replicating latent phase (1). However, this standard curative treatment has no impact on various drug-resistant bacteria, including multidrug-resistant (MDR) and extensively drug-resistant (XDR) *M. tuberculosis*, which not only lengthen the treatment duration but also cause nearly 50% mortality in treated individuals (2).

Therefore, new antituberculosis drugs with novel modes of action are urgently needed. Antituberculosis agents in current development trigger a large panel of biological pathways, such as cell wall synthesis, protein synthesis, or membrane energy production. The number of TB drugs in preclinical and clinical development today is higher than that during the past 40 years. DprE1 is a membrane-associated protein that has been targeted by a diverse set of compounds. Currently, three DprE1 inhibitors have entered clinical trials, including one noncovalent inhibitor, TBA7371, and two covalent inhibitors, BTZ043 and PBTZ169. Nitrobenzothiazinone (BTZ) is one of the most promising scaffolds in the antitubercular drug pipeline and is active against tubercle bacilli at nanomolar concentrations *in vitro* (3–6). BTZ efficiently prevents *M.*

Received 19 November 2017 Returned for modification 23 January 2018 Accepted 27 March 2018

Accepted manuscript posted online 23 April 2018

Citation Xiong L, Gao C, Shi Y-J, Tao X, Peng C-T, Rong J, Liu K-L, Lei Q, Zhang Y-W, Wang N-Y, Yu L-T. 2018. Metabolism of SKLB-TB1001, a potent antituberculosis agent, in animals. *Antimicrob Agents Chemother* 62:e02375-17. <https://doi.org/10.1128/AAC.02375-17>.

Copyright © 2018 American Society for Microbiology. All Rights Reserved.

Address correspondence to Ning-Yu Wang, ningyuwang_sklb@scu.edu.cn, or Luo-Ting Yu, yuluot@scu.edu.cn.

L.X. and C.G. contributed equally to this article.

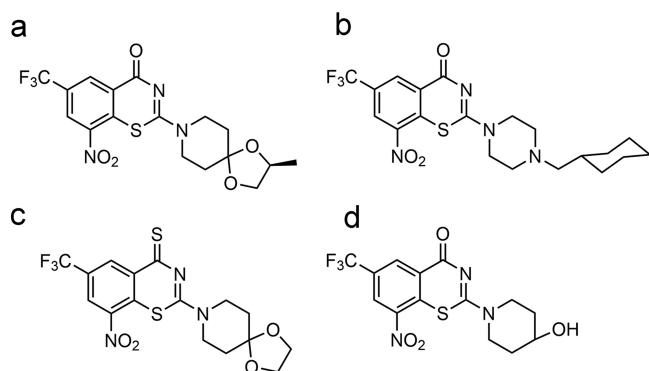


FIG 1 Structures of BTZ043 (a), pBTZ169 (b), SKLB-TB1001 (c), and M4-NO₂ (d).

tuberculosis cell wall synthesis by inhibiting DprE1, which is essential for the synthesis of D-arabinofuranose, a component of arabinogalactan and arabinomannan (7–9). The most promising nitrobenzothiazinone, pBTZ169 (Fig. 1b), is undergoing phase II clinical trials (<http://www.newtdrugs.org/pipeline/clinical>).

We recently reported a new benzothiazinethione, SKLB-TB1001, which had promising antitubercular potency against drug-sensitive, as well as MDR and XDR, *M. tuberculosis in vitro* at nanomolar concentrations. In addition, additive to synergistic interactions were observed when SKLB-TB1001 was combined with other TB drugs in checkerboard assays (10, 11). However, although SKLB-TB1001 showed excellent antitubercular efficacy *in vitro*, it was less effective in a murine model in further studies. The unsatisfactory effects *in vivo* are consistent with the results for BTZ043 (Fig. 1a), which only reduced the bacterial burden in the lungs and spleens by 1 and 2 logs, respectively, after 4 weeks of treatment at a dose 37.5 mg/kg; BTZ043 was thus less potent than expected from *in vitro* studies (3).

Elucidation of the novel mechanism accounting for this phenomenon will contribute to lead optimization of this very promising scaffold and profoundly influence downstream studies. Considering that absorption, distribution, metabolism, and excretion (ADME) always dramatically influence drug potency *in vivo*, the pharmacokinetics (PK) of orally administered SKLB-TB1001 and BTZ043 were analyzed. The moderate elimination half-life ($t_{1/2}$ = 1.45 h for SKLB-TB1001 and 1.22 h for BTZ043) indicated the high correlation between the attenuated potency *in vivo* and their poor ADME profiles (10). Here, we investigated the biotransformation and metabolic pathways of SKLB-TB1001 in animals. In addition, the metabolic by-products were identified by mass spectrometry (MS) and further confirmed by chemical synthesis. The kinetic parameters of the main metabolites were also studied. In addition, these findings identified the common metabolic pathways of BTZs *in vivo* and represent important contributions to the BTZ development process given the structure similarity between SKLB-TB1001 and BTZs.

RESULTS

Pharmacokinetics of SKLB-TB1001. Oral administration of 5 mg/kg SKLB-TB1001 resulted in rapid absorption that reached 150 ng/ml at 0.833 h (Table 1; and see also Fig. 6b). Comparison of the peroral (p.o.) area under the concentration-time curve (AUC) with the intravenous (i.v.) AUC of SKLB-TB1001 in plasma over time showed an apparent oral bioavailability of 44.4% (50-mg/kg dose), which was significantly higher than that of BTZ043 (F = 29.5%) (10). These results indicated that SKLB-TB1001 had adequate PK properties for *in vivo* efficacy. The terminal $t_{1/2}$ was 1.45 h, indicating rapid biotransformation of SKLB-TB1001 *in vivo* (Table 1). In addition, the low lung/plasma ratio (0.255 at 0.25 h, 0.365 at 4 h, and 0.376 at 8 h) suggested moderate enrichment of SKLB-TB1001 in the lungs (Fig. 6a and Table 2; see also Table S1 in the supplemental material).

Pharmacokinetics of metabolites after administration of SKLB-TB1001. Initially, we performed full-scan LC-UV spectrometry analysis using the plasma extracts from

TABLE 1 PK parameters after p.o. and i.v. doses of SKLB-TB1001 (5 mg/kg) in male SD rats^a

Administration	PK parameter	U	Value	SD	CV (%)
p.o., 5 mg/kg	T_{max}	h	0.833	1.01	121
	C_{max}	ng/ml	151	82.5	54.6
	AUC_{last}	h · ng/ml	586	422	72.1
	AUC_{INF}	h · ng/ml	847	NA	NA
	Terminal $t_{1/2}$	h	1.45	NA	NA
	F	%	31.5	22.6	71.8
i.v., 5 mg/kg	AUC_{last}	h · ng/ml	1874	263	14.01
	AUC_{INF}	h · ng/ml	1909	279	14.62
	Terminal $t_{1/2}$	h	1.41	0.13	9.27
	V_{ss}	Liters/kg	4.64	0.21	4.48
	CL	Liters/h/kg	2.66	0.39	14.74
	MRT	h	1.77	0.18	10.32

^aNA, not available (the PK parameter was not reported because the terminal phase could not be precisely determined). CV, coefficient of variation; p.o., peroral; i.v., intravenous. $n = 3$ /time point.

mice after an oral dose of SKLB-TB1001, and three metabolite (M1, M2, and M7) peaks were detected, indicating they were primary metabolites in plasma (Fig. 2). The pharmacokinetic parameters of M7 were determined after p.o. administration and i.v. injection of SKLB-TB1001 (Table 3). The time to reach the peak concentration (T_{max}) of M7 was 0.5 h after oral administration. It was the predominant metabolite (approximately 10% of the parent exposure) with an extremely high level in plasma after either oral or intravenous administration. The concentrations of M1 to M6 were <10% of the parent exposure in mouse plasma.

Identification of metabolites. We generated liquid chromatography-mass spectrometry (LC-MS) extracted ion chromatograms (EICs) of SKLB-TB1001 and its metabolites in plasma samples (Fig. 3). SKLB-TB1001 formed $[M+H]^+$ at m/z 434 in positive-ion scan mode, and the fragment ions of SKLB-TB1001 were mainly observed at m/z 352 in the product-ion scan at m/z 535. Then, a precursor-ion scan at m/z 352 was performed, and seven metabolites, M1 to M7, were detected in mouse plasma (Table 4; see also Fig. S2 in the supplemental material).

For M1, the tandem MS (MS/MS) spectrum in positive mode yielded prominent fragment ions at m/z 362, 290, and 263, as well as a pseudomolecular ion at m/z 538. Metabolite M1 had a pseudomolecular peak of 176 Da greater than that for M4, indicating a glucuronic acid conjugate of M4. The fragment ion m/z 362 was formed by loss of glucuronic acid from the pseudomolecular ion. Further loss of piperidin-4-ol formed fragment m/z 263.

M2 was identified as the glucuronidation product of M7 (nitro reduction product of the parent), with an observed m/z value of 580 and a mass shift of +176 from M7. M2 yielded fragments at m/z 404, 290, and 263 in the MS/MS spectra, indicating that nitro reduction and glucuronidation occurred on the parent compound. Furthermore, the key fragment m/z 83 was formed by the destruction of 1,3-dioxolane, indicating that the parental moiety was not transformed.

For M3, the MS/MS spectrum in positive mode yielded prominent fragment ions at m/z 274, 247, and 83, as well as a pseudomolecular ion at m/z 388. M3 was identified as a shift of sulfur to oxygen and nitro reduction product of the parent, with an observed m/z value of 388 and a mass shift of -16 from M7 (nitro reduction product

TABLE 2 PK parameters for SKLB-TB1001 after administration of a 50-mg/kg p.o. dose of SKLB-TB1001 in male CD1 mice

Site	T_{max} (h)	C_{max} (ng/ml)	AUC_{last} (h · ng/ml)	AUC_{INF} (h · ng/ml)	Terminal $t_{1/2}$ (h)
Plasma	4.00	730	6112	6121	2.46
Lung	4.00	275	1509	NA	NA

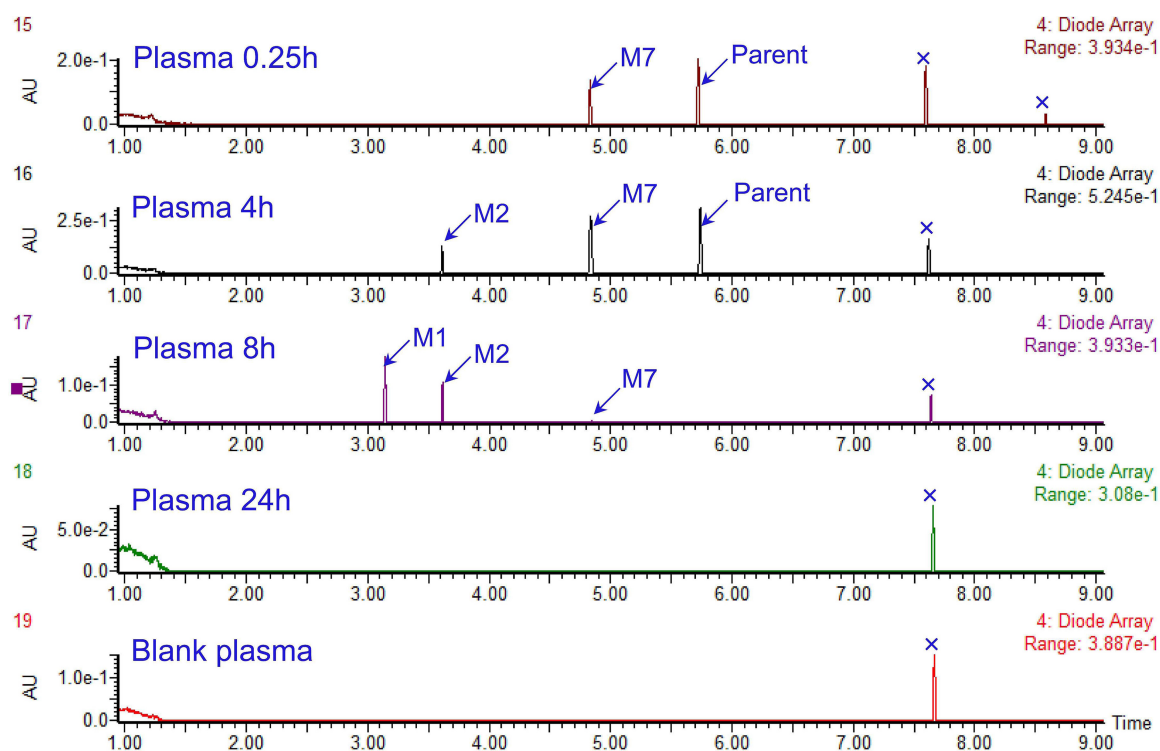


FIG 2 LC-UV chromatograms (337 to 376 nm) of plasma samples from mice at 0.25, 4, 8, and 24 h postdosing and control plasma.

of the parent). M3 also yielded fragments at m/z 83 in the MS/MS spectra, indicating an unbroken structure of 1,3-dioxolane.

The MS/MS spectrum in the positive mode of M4 gave prominent fragment ions at m/z 290, 263, and 100, as well as a pseudomolecular ion at m/z 362. We observed that a loss of glucuronic acid from M1 produces M4, given that many of the same fragment ions appeared on their spectra, including the key fragments m/z 362, 290, 263, and 100. The fragment ion m/z 100 further indicated that the parental moiety has been transformed into piperidin-4-ol through O-dealkylation.

For M5, the MS/MS spectrum in positive mode yielded prominent fragment ions at m/z 279, 306, and 83, as well as the pseudomolecular ion at m/z 420. M5 was identified as the hydroxylation product of M7 with an observed m/z value of 420 and a mass shift of +16 from M7. It also yielded fragments at m/z 83 in the MS/MS spectra, indicating an unbroken structure of 1,3-dioxolane.

The MS/MS spectrum in the positive mode of M6 gave prominent fragment ions at m/z 304, 277, and 83, as well as the pseudomolecular ion at m/z 418. M6 was identified as a product with replacement of sulfur by oxygen in SKLB-TB1001 with an observed m/z value of 418 and a mass shift of -16 from the parent compound. The loss of 1,4-dioxo-8-azaspiro[4.5]decane of M6 led to the fragment m/z 277.

TABLE 3 PK parameters of M7 after a 5-mg/kg i.v. or p.o. dose of SKLB-TB1001 in male SD rats

PK parameter	U	Value		SD		CV (%)	
		i.v.	p.o.	i.v.	p.o.	i.v.	p.o.
T_{max}	h	0.417	0.50	0.144	0.00	34.6	0.00
C_{max}	ng/ml	70.6	17.9	25.0	13.5	35.4	75.2
AUC_{last}	h · ng/ml	163	62.8	21.3	46.8	13.1	74.6
AUC_{INF}	h · ng/ml	167	94.0	21.2	NA	12.7	NA
Terminal $t_{1/2}$	h	1.53	1.84	0.108	NA	7.05	NA

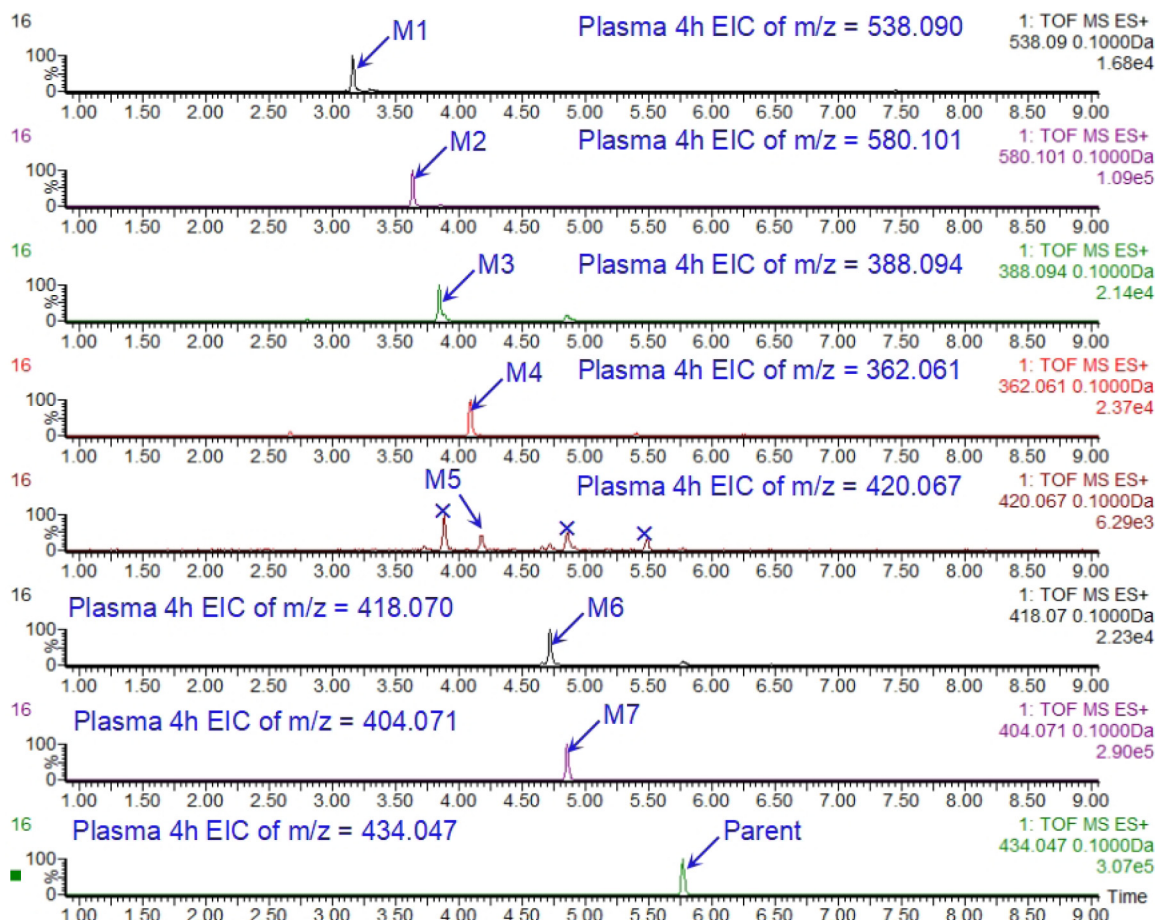


FIG 3 LC-MS extracted ion chromatograms (EICs) of SKLB-TB1001 and its metabolites in plasma samples.

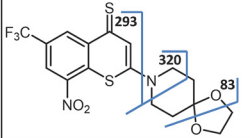
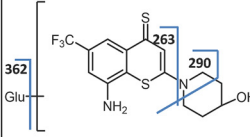
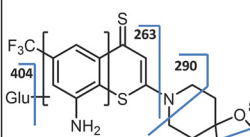
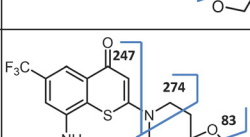
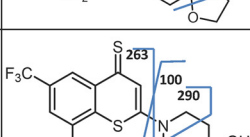
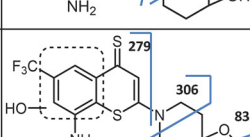
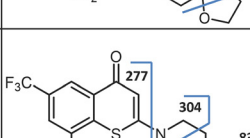
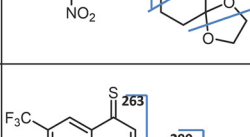
Finally, for M7, the MS/MS spectrum in the positive mode showed prominent fragment ions at m/z 290, 263, and 83, as well as the pseudomolecular ion at m/z 404. M7 was identified as a nitro reduction of SKLB-TB1001 with an observed m/z value of 404 and a mass shift of -30 from the parent compound.

The chemical structures of these metabolites were determined by matching retention times (Fig. 4), parent m/z ions (Fig. 4), and MS/MS fragmentation patterns (see Fig. S2 in the supplemental material) with those of the authentic compounds. In addition, the outcome verified our speculation for M1 to M7.

Antibacterial activity of metabolites. The abilities of the metabolites to inhibit *M. tuberculosis* H37Rv and H37Ra *in vitro* are presented in Table 5. Metabolite M6 had an MIC of $0.07 \mu\text{g/ml}$ *in vitro*. We further performed pharmacokinetic analysis of M6 to determine whether it plays an antibacterial role *in vivo* following oral administration of SKLB-TB1001 (Fig. 5). No trace of M6 was detected in plasma after a 5-mg/kg oral dose of SKLB-TB1001. Even when the dose was increased to 50 mg/kg, the peak concentration (C_{max}) values of M6 in the plasma and lungs were as low as 25.7 ng/ml and 16.8 ng/g, respectively, much lower than the value of its MIC (Fig. 6a and Table 6; see also Table S2 in the supplemental material). In addition, M4-NO₂ (Fig. 1d) also showed anti-TB activity with an MIC of $0.04 \mu\text{g/ml}$.

Effect on cytochrome p450 (CYP450) and plasma protein binding (PPB) study. We selected five human CYP450 isoforms—CYP1A2, CYP2C9, CYP2C19, CYP2D6, and CYP3A4—in the inhibitory test and found that no significant inhibitory effects of both SKLB-TB1001 and pBTZ169 were observed on the five screened CYPs (Table 7). Moreover, no obvious time-dependent CYP inhibition of SKLB-TB1001 could be detected (Table 8), which means SKLB-TB1001 cannot form covalent bonds with CYPs to inhibit

TABLE 4 Identified metabolites of SKLB-TB1001

Compound	Retention time (min)	Formula	MW	Structure
SKLB-TB1001	5.75	C ₁₇ H ₁₅ F ₃ N ₂ O ₄ S ₂	434	
M1	3.11	C ₂₁ H ₂₅ F ₃ N ₃ O ₄ S ₂	538	
M2	3.65	C ₂₃ H ₂₇ F ₃ N ₂ O ₅ S	580	
M3	3.85	C ₁₇ H ₁₇ F ₃ N ₂ O ₃ S	388	
M4	4.11	C ₁₅ H ₁₅ F ₃ N ₂ OS ₂	362	
M5	4.19	C ₁₈ H ₂₁ F ₃ N ₂ O ₃ S ₂	420	
M6	4.72	C ₁₇ H ₁₅ F ₃ N ₂ O ₅ S	418	
M7	4.87	C ₁₇ H ₁₇ F ₃ N ₂ O ₂ S ₂	404	

CYP activity. These results indicated that SKLB-TB1001 caused little hepatotoxicity, and there was a low probability of drug-drug interactions in the concomitant treatment.

The *in vitro* protein binding of SKLB-TB1001 and pBTZ169 in mouse and human sera is shown in Table 9. High protein binding was confirmed. The PPB values of SKLB-TB1001 in human plasma and in CD-1 mouse plasma samples were approximately 99.4 and 96.2%, respectively. No obvious interspecies differences were observed for SKLB-TB1001 and pBTZ169.

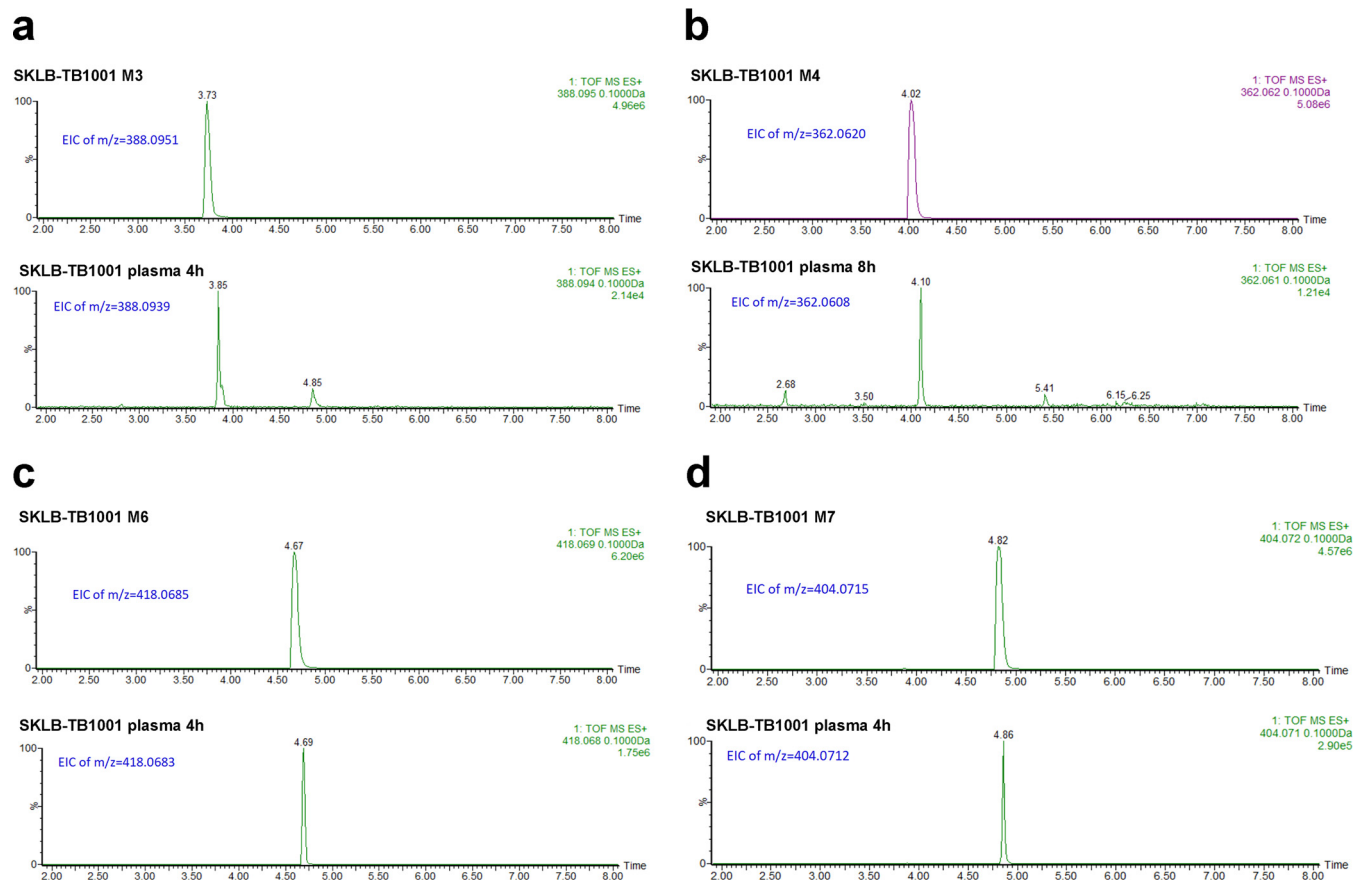


FIG 4 LC-MS EICs of SKLB-TB1001 metabolites for the synthesized standard and in mouse plasma. (a) LC-MS EIC of M3 of the synthesized standard (retention time [RT] = 3.73 min) and in mouse plasma (RT = 3.85 min); (b) LC-MS EIC of M4 for the synthesized standard (RT = 4.02 min) and in mouse plasma (RT = 4.10 min); (c) LC-MS EIC of M6 for the synthesized standard (RT = 4.67 min) and in mouse plasma (RT = 4.69 min); (d) LC-MS EIC of M7 for the synthesized standard (RT = 4.82 min) and in mouse plasma (RT = 4.86 min).

Stability in microsome assays. The stabilities of SKLB-TB1001, M6 (activated metabolite), and M7 (main metabolite) in microsomes were also profiled (Table 10). SKLB-TB1001 showed moderate metabolic stability in human liver microsomes (elimination $t_{1/2}$ = 30.96 min; intrinsic clearance $[CL_{int}]$ = 56.14 ml/min/kg), rat liver microsomes (elimination $t_{1/2}$ = 19.42 min; CL_{int} = 127.94 ml/min/kg), and mouse liver microsomes (elimination $t_{1/2}$ = 22.14 min; CL_{int} = 246.51 ml/min/kg) microsomes. Poor stability in microsomes of M7 can be confirmed by a high clearance rate and a short half-life, whereas good stability across all three species could be indicated by the elimination $t_{1/2}$ in the presence of human liver microsomes (61.4 min), rat liver microsomes (100.9 min), and mice liver microsomes (104.7 min) of M6.

TABLE 5 MICs for metabolites, M4-NO₂, and SKLB-TB1001

Compound	MIC (H37Rv), μ g/ml
SKLB-TB1001	0.02
M1	>50
M2	>50
M3	>50
M4	>50
M5	>50
M6	0.07
M7	>50
M4-NO ₂	0.04 ^a
RMP	0.04

^aThat is, the MIC value against *M. tuberculosis* H37Ra.

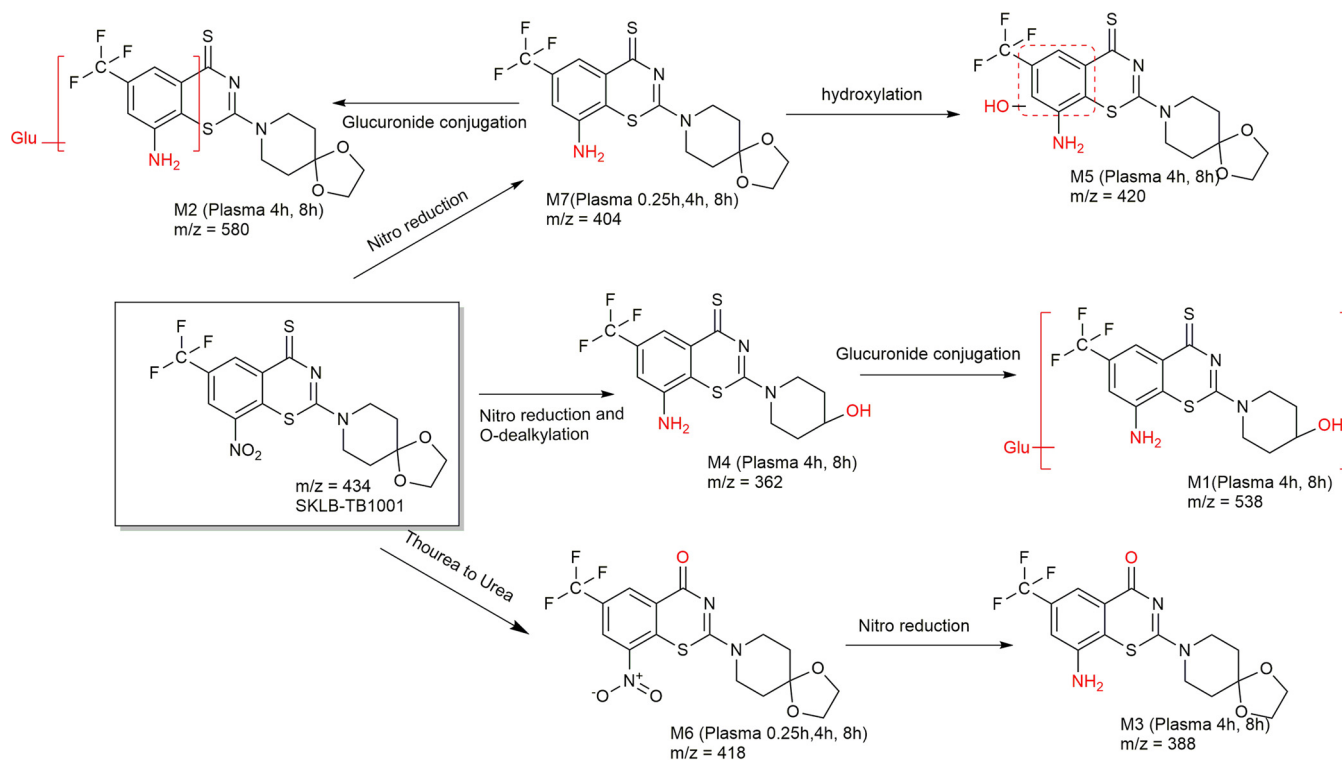


FIG 5 Metabolic pathway of SKLB-TB1001 *in vivo*.

DISCUSSION

The mechanism of biotransformation on the BTZ nitroaromatic core moiety has been elucidated in previous studies (12), but no explanation has been given for the attenuating drug potency *in vivo*. Here, the identification and characteristics of metabolites of the DprE1 inhibitor SKLB-TB1001 following oral administration in mice were reported. The metabolic pathways of SKLB-TB1001 in mouse plasma were profiled based on these findings (Fig. 5). SKLB-TB1001 was shown to be metabolized *in vivo* through three metabolic pathways. The first metabolic pathway (pathway 1) is reduction of the nitro group and O-dealkylation of the piperidine moiety (M4), followed by conjugation of glucuronic acid to M1. The second metabolic pathway (pathway 2) is reduction of the nitro group (M7), followed by hydroxylation of the benzene moiety to M5 and conjugation of glucuronic acid to M2. The third pathway (pathway 3) is replacement of sulfur by oxygen (M6), the only metabolite retaining the nitro group, followed by reduction of the nitro group to M3.

Seven metabolites (M1 to M7) were produced in the metabolic pathways. Nitro groups in the 8 position of all metabolites, except M6, were reduced to amino groups. Previous studies have noted the key role of the nitro group in the 8 position (7, 13, 14). At the molecular level, DprE1 reduces the nitro groups of BTZs with FADH₂ as an electron donor to generate electrophiles that react in a near-quantitative manner with the active-site of DprE1 itself and lead to its inactivation (5). Considering these findings, further investigation of the anti-TB activity of metabolites was conducted, which revealed that all amino metabolites did not show activity against H37Rv *in vitro*. Meanwhile, the predominant metabolite M7 was produced rapidly with a T_{max} of 0.5 h after oral administration of SKLB-TB1001, which was earlier than the T_{max} of 0.833 h for SKLB-TB1001. Based on these findings, rapid transformation into many inactive metabolites is one of the reasons for the decrease in SKLB-TB1001 potency *in vivo*.

Because of the high anti-TB activity of metabolite M6, we further conducted a pharmacokinetic analysis of M6 to determine whether it also played an antibacterial role following the oral administration of SKLB-TB1001 (50 mg/kg). The C_{max} M6 and

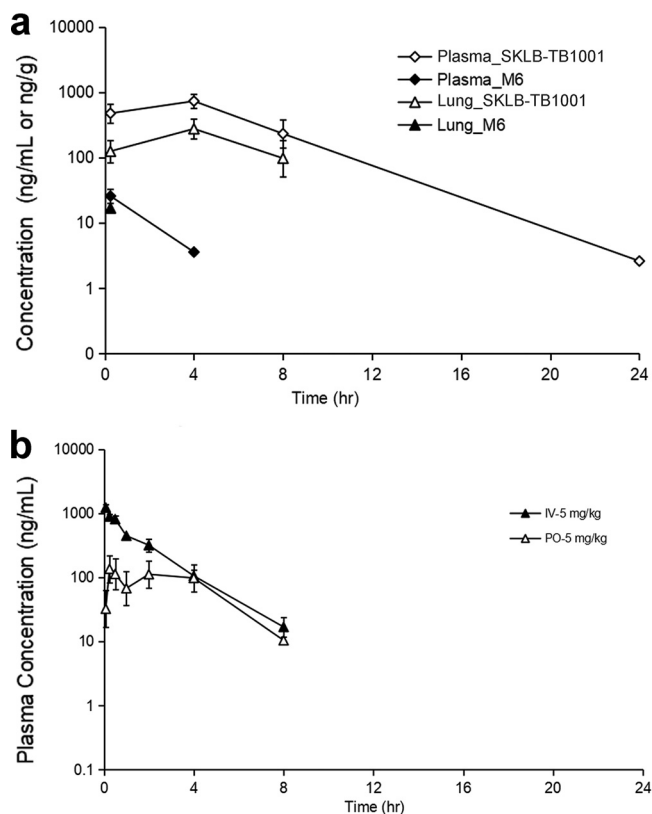


FIG 6 (a) Mean plasma and lung concentration-time profiles of SKLB-TB1001 and its metabolite M6 after a p.o. dose of SKLB-TB1001 at 50 mg/kg in male CD1 mice ($n = 3$ /time point). (b) Mean plasma concentration-time profiles of SKLB-TB1001 after i.v. and p.o. doses in male SD rats ($n = 3$).

C_{max} SKLB-TB1001 values in the plasma and lungs were as low as 3.5 and 6.1%, respectively, indicating that only trace amounts of M6 were produced. Given the short-term presence of M6 in the blood and lung (only detected at 0.25 and 4 h in the plasma and at 0.25 h in the lungs) and the metabolic pathway of M6, we concluded that the M6 metabolite was rapidly transformed into M3 and contributed very little to the anti-TB activity in the SKLB-TB1001 therapeutic strategy.

A high level of PPB of SKLB-TB1001 was one of the major causes of the low lung/plasma ratio (15, 16). Since only unbound drug is in equilibrium across membranes, PPB is an important drug characteristic that has implications for drug function *in vivo*. The high level of protein binding of SKLB-TB1001 resulted in only 0.6 and 3.8% free-drug fractions in human plasma and CD-1 mouse plasma, respectively, which limits

TABLE 6 Individual and mean plasma concentration-time data for metabolite M6 after a 50-mg/kg p.o. dose of SKLB-TB1001 administered to male CD1 mice^a

Location	Sampling time (h)	Mean concn (ng/ml)	SD	CV (%)	Lung/plasma ratio
Plasma	0.25	25.7	7.60	29.6	0.960
	4	3.57	NA	NA	0.960
	8	BQL	NA	NA	0.960
	24	BQL	NA	NA	0.960
Lung	0.25	16.8	NA	NA	0.960
	4	BQL	NA	NA	0.960
	8	BQL	NA	NA	0.960
	24	BQL	NA	NA	0.960

^aBQL, below the quantifiable limit of 3.00 ng/ml for SKLB-TB1001 and M6 in mouse plasma and lung homogenate. NA, not available.

TABLE 7 Results of CYP450 inhibition test

Compound	Inhibition of CYP (IC ₅₀ , μ M)				
	1A2	2C9	2C19	2D6	3A4
SKLB-TB1001	>10	>10	>10	>10	>10
pBTZ169	>10	>10	>10	>10	>10

the lung drug concentration through steady-state equilibrium with plasma. At this point, we deduced that sequestration of the drug by PPB also contributes to the effective attenuation of SKLB-TB1001 potency *in vivo*.

Important information about the structure and groups of SKLB-TB1001 was provided by metabolic research, which is helpful and valuable for the design and structural modification of this drug. PBTZ169 and BTZ043 were reported to show similar pharmacokinetic properties. Makarov et al. (6) evaluated the nitroreduction effect of BTZ043 and PBT169 using NfnB assays, which is an effective way to confirm the nitroreduction. Our study of SKLB-TB1001 further confirmed the existence of nitroreduction metabolites *in vivo*. Considering the similarities in the structure and mechanism of SKLB-TB1001, BTZ043, and PBTZ169, nitroreduction also may occur during the metabolism of BTZ043 and PBTZ169. In addition, the metabolic pathways of SKLB-TB1001 can act as an important reference for BTZ043 because of their similarities on the indicated chain. Meanwhile, reversible reduction on the benzene ring of BTZ043 was reported to occur in all mammalian species investigated. Considering the similar electron density between the oxygen atom and sulfur atom, this reduction may occur on SKLB-1001. However, only trace transformation of sulfur atoms to oxygen atoms of SKLB-1001 *in vivo* was observed. This phenomenon indicated that the sulfur atom may have a special effect on the potency of SKLB-1001. The results showed that reduction of the nitro group leads to decreased potency of BTZs *in vivo*; thus, modification strategies to prevent this reduction, such as a bulk and electron-donating group introduction in the vicinity of the nitro group, may be an effective way to improve drug potency *in vivo*. The replacement of the nitro group by an azide group yielded a new an effective reversible and noncovalent inhibitor of DprE1 (17), which suggested that appropriate replacement of the metabolized groups could maintain the anti-TB activity of this drug. PBTZ169 was indeed more resistant than BTZ043 to nitroreduction by NfnB (6) and showed improved potency *in vivo*. Given this phenomenon and our study, modification strategies for next new series of BTZs should be developed to prevent the reduction. In most metabolites, the side chain of SKLB-TB1001 was converted to hydroxypiperidine; thus, the MIC of M4-NO₂, which has both a hydroxypiperidine group and a nitro group, was determined. M4-NO₂ exhibited a low MIC of 0.04 μ g/ml for H37Ra, which suggested the identification of more optimized compounds for targeting DprE1.

The liver enzymatic complex of cytochrome P450 is engaged in the metabolism of drugs of different chemical structures and pharmacological groups, including antibacterial agents (18). Since comorbidity (TB/HIV) and concomitant medications are common in pulmonary TB patients, pharmacokinetic interactions between different drugs at the level of cytochrome P450 may occur (19, 20). The *in vitro* study of CYP isoforms showed a weak inhibitory effect and low percent time-dependent CYP inhibition (TDI) of SKLB-TB1001 on the activities of the CYP1A2, CYP2C9, CYP2C19, CYP2D6, and

TABLE 8 Percent TDI values for SKLB-TB1001

Compound/isoform ^a	TDI (%) ^b				
	1A2	2C9	2C19	2D6	3A4
SKLB-TB1001	5.48	0.00	8.46	0.00	13.34
Reference	79.82	72.64	81.65	73.17	69.85

^aReference inhibitors: furafylline for CYP1A2, tienilic acid for CYP2C9, ticlopidine for CYP2C19, mifepristone for CYP3A4, and paroxetine for CYP2D6.

^bTime-dependent CYP inhibition (TDI) is normalized based on the enzyme activity at 0 min of preincubation. If the calculated TDI is <0, then the TDI is 0.

TABLE 9 Results of plasma protein binding tests

Compound	Specificity	% unbound (<i>n</i> = 3)	% bound
SKLB-TB1001	Human plasma	0.6	99.4
	CD-1 mouse plasma	3.8	96.2
pBTZ169	Human plasma	0.4	99.6
	CD-1 mouse plasma	0.2	99.8
Warfarin	Human plasma	1.0	99.0
	CD-1 mouse plasma	4.3	95.7

CYP3A4 isoforms. The potential risks of drug interactions are low for the use of SKLB-TB1001 for latent TB treatment in HIV-infected patients receiving protease inhibitor-based antiretroviral therapy with a lack of significant inhibition of CYP450. Like BTZ043 and PBTZ169, SKLB-TB1001 showed moderate metabolic stability in human liver microsomes, indicating a fast transformation of SKLB-TB1001 in liver microsomes. Then, the metabolic stabilities in human liver microsomes of major metabolite M7 and active metabolite M6 were further determined. M6 showed excellent stability in human liver microsomes. This result further confirmed the value of M6 as a new lead compound.

In conclusion, based the obtained metabolic results for SKLB-TB1001, four factors were shown to be closely related to the potency decrease of SKLB-TB1001 in a chronic model. They were (i) a rapid transformation into inactive metabolites of SKLB-TB1001, (ii) a low drug load in lungs, (iii) a rapid transformation of the active metabolite M6, and (iv) high levels of SKLB-TB1001 PPB. All of these results can provide important information for the further structural design and modification of SKLB-1001.

MATERIALS AND METHODS

Materials. SKLB-TB1001 and related compounds used in this study were provided by the State Key Laboratory of Biotherapy, Sichuan University. The mice and Sprague Dawley rats (SD rats) used here were obtained from Beijing HFK Bioscience Co., Ltd. (Beijing, China). The NADPH regenerating system solutions A and B and recombinant human CYP450 were obtained from Corning (Woburn, MA). *Mycobacterium* strains H37Rv and H37Ra were maintained at the University of Illinois in Chicago.

Pharmacokinetic study. All animal experiments were approved by the Institutional Animal Care and Treatment Committee of Sichuan University in China and carried out in accordance with the approved guidelines. SD rats and mice were used in the pharmacokinetic study. Every treatment group contained three rats. Rats and mice were dosed with a SKLB-TB1001 suspension at 5 or 50 mg/kg (i.v. and p.o.). Compounds were dissolved in 5% dimethyl sulfoxide (DMSO)–10% Solutol HS15 in saline for intravenous injection and suspended in 0.5% CMC for oral administration. Blood was collected from the jugular vein of each animal at the following times after drug administration: 0.083, 0.25, 0.5, 1, 2, 4, 6, 8, and 24 h after a single i.v. dosing for SD rats; 0.083, 0.25, 0.5, 1, 2, 4, 6, 8, and 24 h after a single p.o. dosing for SD rats; and 0.25, 4, 8, and 24 h after a single p.o. dosing for male SD mice. All blood samples were centrifuged

TABLE 10 Stability in microsomes of SKLB-TB1001, M6, and M7^a

Compound	Species	Mean	
		<i>t</i> _{1/2} (min)	CL _{int} (ml/min/kg)
Ketanserin	Human	44.33	39.21
	Rat	14.26	174.20
	Mouse	21.28	256.41
SKLB-TB1001	Human	30.96	56.14
	Rat	19.41	127.94
	Mouse	22.14	246.51
M6	Human	254.06	6.84
	Rat	50.43	49.25
	Mouse	36.71	148.67
M7	Human	19.48	89.23
	Rat	7.36	337.53
	Mouse	7.93	688.49

^a*n* = 3.

at 3,000 rpm for 10 min to obtain serum, which was then stored at -20°C . Then, $150\ \mu\text{l}$ of the serum was added to $500\ \mu\text{l}$ of acetonitrile, and the mixture was centrifuged at 13,000 rpm for 10 min to remove the protein. The supernatant was dried and dissolved in $100\ \mu\text{l}$ of acetonitrile, and this solution was centrifuged at 13,000 rpm for 10 min.

The supernatant was moved to a sample bottle for HPLC analysis. Total area under the concentration-time curve (AUC), the elimination half-life ($t_{1/2}$), the peak concentration (C_{max}), and the time to reach peak concentration (T_{max}) of samples were determined directly from the experimental data using WinNonlin V6.2.1.

Mouse plasma sample processing (investigation of metabolites). Mouse plasma (p.o., 50 or 5 mg/kg): Aliquots of three mouse plasma samples collected at different times posttreatment were pooled into four samples ($150\ \mu\text{l}$ each) according to the collection time and then combined with $450\ \mu\text{l}$ of acetonitrile (ACN).

All the mixtures were vortexed for 4 min and centrifuged at 14,000 rpm for 5 min. Next, a $580\text{-}\mu\text{l}$ portion of the supernatant from the samples was evaporated under an N_2 stream until dry. The dried extracts were then reconstituted with $150\ \mu\text{l}$ of ACN:H₂O (1:3 [vol/vol]), vortexed for 2 min, and centrifuged at 14,000 rpm for 5 min. Next, $10\ \mu\text{l}$ of the resultant supernatants was directly injected into an LC-UV-MS apparatus. The LC-UV-MS conditions are presented in Tables S3 and S4 in the supplemental material.

M. tuberculosis H37Rv MIC assay. The MICs against *M. tuberculosis* H37Rv and H37Ra were determined by using a microplate alamarBlue assay (21). Compounds were dissolved in DMSO at concentrations of 32 to $0.008\ \mu\text{g/ml}$. *M. tuberculosis* was grown to late log phase in Middlebrook 7H9 medium supplemented with 0.05% Tween 80, 0.2% (vol/vol) glycerol, and 10% (vol/vol) oleic acid-albumin-dextrose-catalase. The cultures were then centrifuged, washed, and resuspended in phosphate-buffered saline. Suspensions were filtered through an $8\text{-}\mu\text{m}$ -pore-size filter. Aliquots were then frozen at -80°C . The CFU number was determined by plating on 7H11 agar plates. Twofold dilutions of compounds were prepared in Middlebrook 7H12 medium in a volume of $100\ \mu\text{l}$ in 96-well microplates. *M. tuberculosis* ($100\ \mu\text{l}$ inoculum of 10^6 CFU/ml) was added, and the plates were incubated at 37°C . On day 10, $20\ \mu\text{l}$ of 0.01% alamarBlue and $12.5\ \mu\text{l}$ of 20% Tween 80 were added to each well. After 24 h, the fluorescence of each well was measured at an excitation wavelength of 530 nm and an emission wavelength of 590 nm. The MICs were defined as the lowest concentration resulting in a $\geq 90\%$ reduction in fluorescence relative to the controls. The reported MICs are an average of two or three individual measurements.

PPB determination. The extent of PPB for each test compound was determined by equilibrium dialysis (22). A 96-well rapid equilibrium dialysis (RED) kit (Thermo Fisher Scientific) with cassettes of compounds (pooling of compounds predialysis) was used to perform the analysis (each run was performed in triplicate). The plasma was centrifuged (4 min, 3,500 rpm) and adjusted to pH 7.4 to pH 7.5 with 1% phosphoric acid and 1 N sodium hydroxide. The test compound was added to the plasma, which was then mixed and heated ($1\ \mu\text{M}$, 1% [vol/vol] DMSO, 37°C). Regenerated cellulose membranes (5,000 Da; Harvard Apparatus) were soaked in phosphate buffer for 5 min and placed in a Fast Micro-Equilibrium dialyzer (Harvard Apparatus). Subsequently, the plasma containing compounds was added to the donor side of the single-use RED plate. Buffer was added to the other side. Equilibrium dialysis was undertaken by incubation (18 h, 37°C), and samples were removed from each compartment for LC-MS/MS analysis.

Inhibition to cytochrome P450. The CYP inhibitory potential of SKLB-TB1001 and pBTZ169 was determined using the following recombinant microsomes (23): CYP1A2, CYP2C9, CYP2C19, CYP2D6, and CYP3A4. Each incubation reaction mixture (T0, T5, T20, T30, T60, and NCF60), which contained recombinant microsomes ($80\ \mu\text{l}$), compounds ($10\ \mu\text{l}$), and extra phosphate buffer (100 mM, pH 7.4), was added in NCF60. Incubation mixtures were preincubated at 37°C for 5 min. After incubation, 25 ml of NADPH regenerating system solution was added to each well, and reactions were started immediately at 37°C . The reactions were terminated with $300\ \mu\text{l}$ after 60 min of terminal solution (tolbutamide, 100 ng/ml; labetalol, 100 ng/ml). After centrifugation, the supernatant was analyzed by LC-MS/MS.

Time-dependent CYP inhibition. Time-dependent CYP inhibition of SKLB-TB1001 was determined using the recombinant microsomes CYP1A2, CYP2C9, CYP2C19, CYP2D6, and CYP3A4 by single point suppression. The incubation mixtures for a 0-min time point contained $78\ \mu\text{l}$ of $1.3\times$ human liver microsomes (HLM) solution or recombinant CYP2C19 plus $1\ \mu\text{l}$ of $100\times$ reference inhibitor, test compounds, or solvent control, and the incubation mixture for a 30-min time point contained $78\ \mu\text{l}$ of $1.3\times$ HLM solution or recombinant CYP2C19 plus $1\ \mu\text{l}$ of $100\times$ reference inhibitor, test compounds, or solvent control. Incubation mixtures were preincubated at 37°C for 10 min. For the 0-min time point sample, $21\ \mu\text{l}$ of K buffer was added to the corresponding wells that contained $79\ \mu\text{l}$ of enzyme/compound mixture and mixed well. Then, an aliquot of $20\ \mu\text{l}$ was immediately transferred to the secondary incubation system. After 15 min, an aliquot of $60\ \mu\text{l}$ from the secondary incubation was transferred to $120\ \mu\text{l}$ of ACN that contained internal standard (IS) to stop the reaction. For the 30-min time point sample, $21\ \mu\text{l}$ of the NADPH solution was added to the corresponding wells that contained $79\ \mu\text{l}$ of enzyme/compound mixture and mixed well to start the 30-min preincubation. Then, an aliquot of $20\ \mu\text{l}$ was transferred after 30 min to the secondary incubation system. After 15 min, an aliquot of $60\ \mu\text{l}$ from the secondary incubation was transferred to $120\ \mu\text{l}$ of ACN that contained IS to stop the reaction. Finally, 25 ml of NADPH regenerating system solution was added to each well, and reactions were started immediately at 37°C . After centrifugation, the supernatant was analyzed by LC-MS/MS.

Stability in microsome assay. Previously published incubation procedures using human liver microsomes (HLM), rat liver microsomes (RLM), and mice liver microsomes (MLM) were used with modifications. First, $10\ \mu\text{l}$ of 10 mM DMSO stock solution was added to $190\ \mu\text{l}$ of ACN to prepare 500 μM spiking solution. Then, $1.5\ \mu\text{l}$ of 500 μM spiking solution and $18.75\ \mu\text{l}$ of 20-mg/ml liver microsomes were added to $479.75\ \mu\text{l}$ of buffer on ice to prepare 5 μM spiking solution in microsomes (0.75 mg/ml).

Next, 30 μl of 1.5 μM spiking solution containing 0.75 mg/ml microsome solution was added to the assay plates designated for different time points (0, 5, 15, 30, and 45 min) on ice. For 0 min, 135 μl of ACN containing IS was added to the wells of the 0-min plate, and then 15 μl of NADPH stock solution (6 mM) was added. The compounds were preincubated with microsome solution for 5 min at 37°C, followed by a 45-min incubation at 37°C with the substrates (15 μl NADPH). At 5, 15, 30, and 45 min, 135 μl of ACN containing IS was added to the wells of corresponding plates, respectively, to stop the reaction. After quenching, the plates were shaken using a vibrator (IKA, MTS 2/4) for 10 min (600 rpm/min) and then centrifuges at 5,594 $\times g$ for 15 min (Thermo Multifuge \times 3R). Next, 50 μl of the supernatant was transferred from each well into a 96-well sample plate containing 50 μl of ultrapure water (Millipore, catalog no. ZMQS50F01) for LC-MS analysis.

Synthesis of compounds. (i) **8-Nitro-2-(1,4-dioxo-8-azaspiro[4,5]decan-8-yl)-6-(trifluoro-methyl)-4H-thiochromen-4-one (M6).** For the generation of 10 g of 2-chloro-3-nitro-5-(trifluoromethyl) benzoic acid in dichloromethane, 8 ml of oxalyl chloride and 0.2 ml *N,N*-dimethylformamide (DMF) were added. After stirring for 3 h at room temperature, the solvent was removed under reduced pressure and redissolved in 25 ml of dry dichloromethane. The mixture and 1 g of 18-crown-6 were added to 8 g of ammonium thiocyanate dropwise. The mixture was then stirred at room temperature for 1.5 h. The reaction mixture was filtered, and the filtrate was added to 6 g of 1,4-dioxo-8-azaspiro[4.5] decane. The reaction mixture was then stirred at room temperature until the starting material was completely consumed as shown by thin-layer chromatography (TLC). After evaporation of the solvent, the residue was purified over silica gel using ethyl acetate-petroleum ether (3:1, vol/vol) as eluent to obtain a yellow product (9.20 g, 59%). $^1\text{H-NMR}$ (400 MHz, Chloroform-*d*) δ 9.10 (d, $J = 2.1$ Hz, 1H), 8.76 (d, $J = 2.1$ Hz, 1H), 4.21 (d, $J = 6.0$ Hz, 2H), 4.03 (s, 6H), 1.87 (s, 4H). $^{13}\text{C-NMR}$ (101 MHz, Chloroform-*d*) δ 166.54, 161.81, 143.94, 134.13, 133.38, 129.67, 126.65, 126.03, 122.30, 106.22, 64.76, 44.69, 35.13. ESI-MS: m/z 418.0685 (M+H) $^+$.

(ii) **SKLB-TB1001.** First, 2 g of M6 and 1.35 g of Lawesson's reagent were suspended in 50 ml of dry toluene. The reaction mixture was refluxed until the starting material was completely consumed, as shown by TLC. Then, the solvent was removed under reduced pressure, suspended in ethyl acetate and methyl alcohol (3:1), and stirred overnight at room temperature. The suspension was filtered to acquire SKLB-TB1001 as a red filter cake (1.64 g, 80%). $^1\text{H-NMR}$ (400 MHz, DMSO-*d*₆) δ 9.26 (d, $J = 2.0$ Hz, 1H), 8.80 (d, $J = 2.1$ Hz, 1H), 4.14 (s, 2H), 3.96 (s, 4H), 3.90 (s, 2H), 1.83 (s, 4H). $^{13}\text{C-NMR}$ (101 MHz, DMSO-*d*₆): δ 166.53, 161.80, 143.92, 134.14, 133.35, 129.66, 126.63, 126.03, 122.38, 106.21, 64.76, 44.68, 35.12. ESI-MS: m/z 456.0 (M+Na) $^+$.

(iii) **8-Amino-2-(1,4-dioxo-8-azaspiro[4,5]decan-8-yl)-6-(trifluoro-methyl)-4H-thiochromen-4-one (M3).** First, 3 g of M6 and 804 mg of ammonium chloride were suspended in a mixed solvent of alcohol, tetrahydrofuran, and distilled water (3/3/1). The reaction was stirred at 60°C for 20 min to obtain a pellucid solution, and 3.25 g (8eq) of iron powder was added to the reaction under strongly stirring conditions. The reaction mixture was heated at 80°C for 1 h. The mixture was filtered, and after evaporation of the solvent, the crude product was purified by silica gel column chromatography (eluent: dichloromethane-methyl alcohol, 20/1) to yield the desired product as a white solid (2.1 g, 75%). $^1\text{H-NMR}$ (400 MHz, DMSO-*d*₆) δ 7.68 (d, $J = 1.9$ Hz, 1H), 7.21 (d, $J = 2.0$ Hz, 1H), 6.04 (s, 2H), 3.95 (s, 4H), 3.92 (s, 4H), 1.79 (d, $J = 6.4$ Hz, 4H). $^{13}\text{C-NMR}$ (101 MHz, DMSO-*d*₆) δ 167.99, 160.67, 145.69, 128.26, 123.71, 120.58, 113.11, 112.12, 112.11, 106.61, 64.51, 34.69. ESI-MS: m/z 388.0915 (M+H) $^+$.

(iv) **8-Amino-2-(1,4-dioxo-8-azaspiro[4,5]decan-8-yl)-6-(trifluoro-methyl)-4H-thiochromen-4-thione (M7).** The synthetic method of M7 was the same as that for SKLB-TB1001. The reactants were M3 and Lawesson's reagent. The desired product was a yellow solid (820 mg, 78%). ESI-MS: m/z 404.0715 (M+H) $^+$. $^1\text{H-NMR}$ (400 MHz, DMSO-*d*₆) δ 8.29 (d, $J = 1.8$ Hz, 1H), 7.21 (d, $J = 1.9$ Hz, 1H), 6.05 (s, 2H), 4.10 (s, 2H), 3.96 (s, 4H), 3.77 (s, 2H), 2.51 (t, $J = 1.9$ Hz, 2H), 1.83 (s, 4H).

(v) **2-(4-Hydroxypiperidin-1-yl)-8-nitro-6-(trifluoromethyl)-4H-thiochromen-4-one (M4-NO₂).** The synthetic method of M4-NO₂ was the same as that for M6, while the side chain moiety was 4-hydroxypiperidine. In addition, the crude product was purified by silica gel column chromatography (eluent: dichloromethane-methyl alcohol, 10/1) to yield M4-NO₂ (9.6 g, 69.3%) as yellow crystals. $^1\text{H-NMR}$ (400 MHz, Chloroform-*d*) δ 9.10 (d, $J = 2.1$ Hz, 1H), 8.76 (d, $J = 2.1$ Hz, 1H), 4.18 (tt, $J = 6.8, 3.5$ Hz, 4H), 3.86 (s, 1H), 2.01 (dd, $J = 9.6, 4.1$ Hz, 2H), 1.79 (s, 2H). $^{13}\text{C-NMR}$ (101 MHz, Chloroform-*d*) δ 166.61, 161.81, 143.95, 134.18, 133.35, 133.31, 126.66, 126.03, 126.00, 69.44, 65.56, 33.71. ESI-MS: m/z 376.0526 (M+H) $^+$.

(vi) **8-Amino-2-(4-hydroxypiperidin-1-yl)-6-(trifluoromethyl)-4H-thiochromen-4-thione (M4).** M4-NO₂ was reduced as described for the synthesis of M3. The reaction mixture was filtered to obtain a brown filtrate. After evaporation of the solvent, the mixture was suspended in 25 ml of dry toluene, and 5.07 g of Lawesson's reagent was added. The reaction mixture was heated to 80°C until the starting material was completely consumed as determined by TLC. After evaporation of the solvent, the mixture was adsorbed onto silica gel and then purified by column chromatography (eluent: dichloromethane-methyl alcohol, 5/1) to yield the desired product as a red solid. (7.63 g, 57.03%). $^1\text{H-NMR}$ (400 MHz, DMSO-*d*₆) δ 11.95 (s, 1H), 8.31 to 8.27 (m, 1H), 7.20 (d, $J = 1.9$ Hz, 1H), 6.04 (s, 2H), 4.96 (d, $J = 3.9$ Hz, 1H), 3.89 (dd, $J = 7.4, 3.8$ Hz, 2H), 1.91 (s, 4H), 1.54 (s, 2H). $^{13}\text{C-NMR}$ (101 MHz, DMSO-*d*₆) δ 200.50, 153.97, 145.67, 129.37, 116.88, 115.91, 111.68, 73.99, 64.96, 63.26, 33.99, 25.41, 24.95. ESI-MS: m/z 362.0620 (M+H) $^+$.

SUPPLEMENTAL MATERIAL

Supplemental material for this article may be found at <https://doi.org/10.1128/AAC.02375-17>.

SUPPLEMENTAL FILE 1, PDF file, 2.0 MB.

ACKNOWLEDGMENTS

This study was supported by the Natural Science Foundation of China (grant 81703570), the China Postdoctoral Science Foundation (2017 M612962), and the National S&T Major Special Project on Major New Drug Innovations (2018ZX09721001).

We thank Yuehong Wang (University of Illinois at Chicago) for providing the MIC data.

REFERENCES

- Villemagne B, Crauste C, Flipo M, Baulard AR, Deprez B, Willand N. 2012. Tuberculosis: the drug development pipeline at a glance. *Eur J Med Chem* 51:1–16. <https://doi.org/10.1016/j.ejmech.2012.02.033>.
- Manjunatha UH, Smith PW. 2015. Perspective: Challenges and opportunities in TB drug discovery from phenotypic screening. *Bioorg Med Chem* 23:5087–5097. <https://doi.org/10.1016/j.bmc.2014.12.031>.
- Makarov V, Manina G, Mikusova K, Mollmann U, Ryabova O, Saint-Joanis B, Dhar N, Pasca MR, Buroni S, Lucarelli AP, Milano A, De Rossi E, Belanova M, Bobovska A, Dianiskova P, Kordulakova J, Sala C, Fullam E, Schneider P, McKinney JD, Brodin P, Christophe T, Waddell S, Butcher P, Albrethsen J, Rosenkrands I, Brosch R, Nandi V, Bharath S, Gaonkar S, Shandil RK, Balasubramanian V, Balganesht T, Tyagi S, Grosset J, Riccardi G, Cole ST. 2009. Benzothiazinones kill *Mycobacterium tuberculosis* by blocking arabinan synthesis. *Science* 324:801–804. <https://doi.org/10.1126/science.1171583>.
- Trefzer C, Rengifo-Gonzalez M, Hinner MJ, Schneider P, Makarov V, Cole ST, Johnsson K. 2010. Benzothiazinones: prodrugs that covalently modify the decaprenylphosphoryl- β -D-ribose 2'-epimerase DprE1 of *Mycobacterium tuberculosis*. *J Am Chem Soc* 132:13663–13665. <https://doi.org/10.1021/ja106357w>.
- Batt SM, Jabeen T, Bhowruth V, Quill L, Lund PA, Eggeling L, Alderwick LJ, Futterer K, Besra GS. 2012. Structural basis of inhibition of *Mycobacterium tuberculosis* DprE1 by benzothiazinone inhibitors. *Proc Natl Acad Sci U S A* 109:11354–11359. <https://doi.org/10.1073/pnas.1205735109>.
- Makarov V, Lechartier B, Zhang M, Neres J, van der Sar AM, Raadsen SA, Hartkoorn RC, Ryabova OB, Vocat A, Decosterd LA, Widmer N, Buclin T, Bitter W, Andries K, Pojer F, Dyson PJ, Cole ST. 2014. Towards a new combination therapy for tuberculosis with next generation benzothiazinones. *EMBO Mol Med* 6:372–383. <https://doi.org/10.1002/emmm.201303575>.
- Abdel-Magid AF. 2015. Decaprenylphosphoryl- β -D-ribose 2'-epimerase 1 (DprE1): a novel therapeutic target for the treatment of tuberculosis. *ACS Med Chem Lett* 6:373–374. <https://doi.org/10.1021/acsmedchemlett.5b00080>.
- Bhutani I, Loharch S, Gupta P, Madathil R, Parkesh R. 2015. Structure, dynamics, and interaction of *Mycobacterium tuberculosis* DprE1 and DprE2 examined by molecular modeling, simulation, and electrostatic studies. *PLoS One* 10:e0119771. <https://doi.org/10.1371/journal.pone.0119771>.
- Breck M, Centarova I, Mukherjee R, Kolly GS, Huszar S, Bobovska A, Kilacskova E, Mocosova V, Svetlikova Z, Sarkan M, Neres J, Kordulakova J, Cole ST, Mikusova K. 2015. DprE1 is a vulnerable tuberculosis drug target due to its cell wall localization. *ACS Chem Biol* 10:1631–1636. <https://doi.org/10.1021/acschembio.5b00237>.
- Gao C, Peng C, Shi Y, You X, Ran K, Xiong L, Ye TH, Zhang L, Wang N, Zhu Y, Liu K, Zuo W, Yu L, Wei Y. 2016. Benzothiazinethione is a potent preclinical candidate for the treatment of drug-resistant tuberculosis. *Sci Rep* 6:29717. <https://doi.org/10.1038/srep29717>.
- Gao C, Ye TH, Peng CT, Shi YJ, You XY, Xiong L, Ran K, Zhang LD, Zeng XX, Wang NY, Yu LT, Wei YQ. 2017. A novel benzothiazinethione analogue SKLB-TB1001 displays potent antimycobacterial activities in a series of murine models. *Biomed Pharmacother* 88:603–609. <https://doi.org/10.1016/j.biopha.2017.01.098>.
- Kloss F, Krchnak V, Krchnakova A, Schieferdecker S, Dreisbach J, Krone V, Mollmann U, Hoelscher M, Miller MJ. 2017. In vivo dearomatization of the potent antituberculosis agent BTZ043 via Meisenheimer complex formation. *Angew Chem Int Ed Engl* 56:2187–2191. <https://doi.org/10.1002/anie.201609737>.
- Piton J, Foo CS, Cole ST. 2017. Structural studies of *Mycobacterium tuberculosis* DprE1 interacting with its inhibitors. *Drug Discov Today* 22:526–533. <https://doi.org/10.1016/j.drudis.2016.09.014>.
- Foo CS, Lechartier B, Kolly GS, Boy-Rottger S, Neres J, Rybniker J, Lupien A, Sala C, Piton J, Cole ST. 2016. Characterization of DprE1-mediated benzothiazinone resistance in *Mycobacterium tuberculosis*. *Antimicrob Agents Chemother* 60:6451–6459. <https://doi.org/10.1128/AAC.01523-16>.
- Trainor GL. 2007. The importance of plasma protein binding in drug discovery. *Expert Opin Drug Discov* 2:51–64. <https://doi.org/10.1517/17460441.2.1.51>.
- Liu L, Collier AC, Link JM, Domino KB, Mankoff DA, Eary JF, Spiekerman CF, Hsiao P, Deo AK, Unadkat JD. 2015. Modulation of P-glycoprotein at the human blood-brain barrier by quinidine or rifampin treatment: a positron emission tomography imaging study. *Drug Metab Dispos* 43:1795–1804. <https://doi.org/10.1124/dmd.114.058685>.
- Tiwari R, Miller AP, Chiarelli L, Mori G, Sarkan M, Centarova I, Cho S, Mikusova K, Franzblau GS, Oliver GA, Miller M. 2016. Design, syntheses, and anti-TB activity of 1,3-benzothiazinone azide and click chemistry products inspired by BTZ043. *ACS Med Chem Lett* 7:266–270. <https://doi.org/10.1021/acsmedchemlett.5b00424>.
- Cao L, Greenblatt DJ, Kwara A. 2017. Inhibitory effects of selected antituberculosis drugs on common human hepatic cytochrome P450 and UDP-glucuronosyltransferase enzymes. *Drug Metab Dispos* 45:1035–1043. <https://doi.org/10.1124/dmd.117.076034>.
- Rae JM, Johnson MD, Lippman ME, Flockhart DA. 2001. Rifampin is a selective, pleiotropic inducer of drug metabolism genes in human hepatocytes: studies with cDNA and oligonucleotide expression arrays. *J Pharmacol Exp Ther* 299:849–857.
- Soars MG, Petullo DM, Eckstein JA, Kasper SC, Wrighton SA. 2004. An assessment of UDP-glucuronosyltransferase induction using primary human hepatocytes. *Drug Metab Dispos* 32:140–148. <https://doi.org/10.1124/dmd.32.1.140>.
- Collins L, Franzblau SG. 1997. Microplate Alamar blue assay versus BACTEC 460 system for high-throughput screening of compounds against *Mycobacterium tuberculosis* and *Mycobacterium avium*. *Antimicrob Agents Chemother* 41:1004–1009.
- Sasahara K, Shimokawa Y, Hirao Y, Koyama N, Kitano K, Shibata M, Umehara K. 2015. Pharmacokinetics and metabolism of delamanid, a novel anti-tuberculosis drug, in animals and humans: importance of albumin metabolism in vivo. *Drug Metab Dispos* 43:1267–1276. <https://doi.org/10.1124/dmd.115.064527>.
- Aggarwal A, Parai MK, Shetty N, Wallis D, Woolhiser L, Hastings C, Dutta NK, Galaviz S, Dhakal RC, Shrestha R, Wakabayashi S, Walpole C, Matthews D, Floyd D, Scullion P, Riley J, Epemolu O, Norval S, Snavelly T, Robertson GT, Rubin EJ, Joerger TR, Sirgel FA, van der Merwe R, van Helden PD, Keller P, Bottger EC, Karakousis PC, Lenaerts AJ, Sacchettini JC. 2017. Development of a novel lead that targets *M. tuberculosis* polyketide synthase 13. *Cell* 170:249–259. <https://doi.org/10.1016/j.cell.2017.06.025>.